Enrichment of (6,5) Single Wall Carbon Nanotubes Using Genomic DNA

Sang N. Kim, Zhifeng Kuang, James G. Grote, Barry L. Farmer, and Rajesh R. Naik*

Materials and Manufacturing Directorate, Air Force Research Laboratory, Wright-Patterson AFB, Ohio 45433

ABSTRACT

Single wall carbon nanotubes (SWNTs) have attracted attention because of their potential in a vast range of applications, including transistors and sensors. However, immense technological importance lies in enhancing the purity and homogeneity of SWNTs with respect to their chirality for real-world electronic applications. In order to achieve optimal performance of SWNTs, the diameter, type, and chirality have to be effectively sorted. Any employed strategy for sorting SWNTs has to be scalable, nondestructible, and economical. In this paper, we present a solubilization and chirality enrichment study of commercially available SWNTs using genomic DNA. On the basis of the comparison of the photoluminescence (PL) and near-infrared absorption measurements from the SWNTs dispersed with salmon genomic DNA (SaDNA) and d(GT)$_{20}$, we show that genomic DNA specifically enriches (6,5) tubes. Circular dichroism and classical all-atom molecular dynamics simulations reveal that the genomic double-stranded SaDNA prefers to interact with (6,5) SWNTs as compared to (10,3) tubes, meanwhile single-stranded d(GT)$_{20}$ shows no or minimal chirality preference. Our enrichment process demonstrates enrichment of >86% of (6,5) SWNTs from CoMoCat nanotubes using SaDNA.

Despite the efforts to obtain chirality-pure single wall carbon nanotubes (SWNTs),[1−8] accomplishing a purification of 99.999%, which is one of the most critical requirements for the application of SWNTs in nanoscale circuits, conductors, electrochemical probes, transistors, and photovoltaic devices, remains a task to be resolved among scientific and industrial communities. For a given nanotube sample, the types of SWNT chirality increase as the mean diameter ($\bar{d}_t$) and diameter distribution (σ) increase. For example, a typical HiPco sample, with $\bar{d}_t = 1.05$ nm and $\sigma = 0.15$ nm, is a mixture of approximately 50 different (n,m)-SWNTs, while the smaller $\bar{d}_t$ sample, such as CoMoCat, contains approximately 25 different (n,m) nanotubes. For most separation protocols so far, the extreme intertube aggregation forces need to be overcome by using an effective surfactant system or nanotube chemical functionalization. By wrapping[2,9] and/or groove-binding[10] with SWNTs via hydrophobic interactions, DNA has been recognized as an efficient SWNT dispersion medium that enables one to obtain both individually exfoliated samples and chirality-fractionated carbon nanotubes according to their diameter (d_t) and metallicity via postsolubilization separation techniques, such as ion exchange[2,11] and density gradient columns.[5] Zheng et al. showed that the single-stranded d(GT)$_{20}$ DNA−oligomer exhibits not only individual-level nanotube dispersion but also effective SWNT chirality separation when eluted from

an anion exchange column at various salt concentrations.[2,11] Apart from DNA as a means to separate SWNT, other methods, such as dielectrophoresis[4] and density gradient ultracentrifugation,[6] have been employed. Strategies for achieving high-purity SWNTs need to be scalable, nondestructive, and economical. Here we present a solubilization and separation study of SWNTs by using a genomic salmon DNA (SaDNA), which is a byproduct of the fishing industry and costs about $20/g (compared to $25000/g for d(GT)$_{20}$). We demonstrate that the SaDNA exfoliates and disperses SWNTs on a level comparable to d(GT)$_{20}$ oligomer DNA. The analysis using near-infrared (NIR) absorption and photoluminescence (PL) spectra from the HiPco nanotube samples shows SaDNA mediates selective stabilization of (6,5) SWNT, without requiring additional separation steps, such as ion exchange[11] and density gradient columns.[5] Circular dichroism and classical all-atom molecular dynamics (MD) simulations show that SaDNA prefers to interact with (6,5) SWNT as compared to (10,3) tubes, whereas single-stranded d(GT)$_{20}$ shows no or minimal chirality preference. Further spectroscopic studies on CoMoCat SWNT−DNA dispersion shows >86% of (6,5) chirality enrichment can be achieved by using SaDNA as the dispersing medium.

HiPco SWNTs have been known to exhibit a $\bar{d}_t$ of 1.05 nm, along with a σ of ±0.15 nm.[12] Such wide σ of the HiPco sample, along with close to 1 nm $\bar{d}_t$ enables us to monitor the metallicity and diameter-dependent stabilization of nanotubes in a dispersion medium by absorption and emission

* To whom correspondence should be addressed, Rajesh.Naik@wpafb.af.mil.
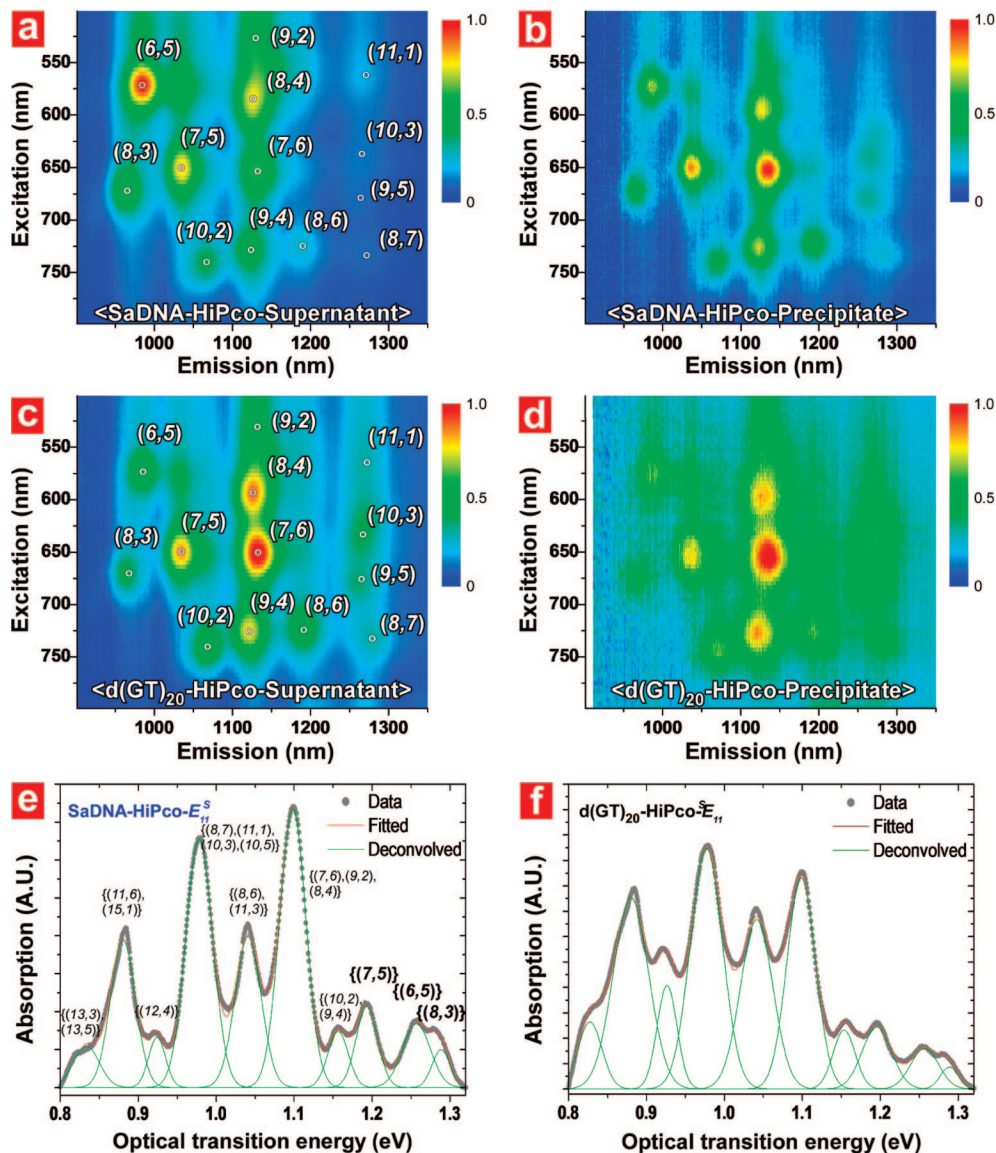
Figure 1. Normalized PLE emission contour plot (a, b) from SaDNA dispersed HiPco SWNTs in the ultracentrifuged supernatant and the redispersed-precipitate fractions, respectively. Normalized PLE emission contour plot (c, d) from $d(GT)_{20}$ dispersed HiPco SWNTs of the ultracentrifugation supernatant and the redispersed-precipitate fractions, respectively. Inset circles added for the visualization of each SWNT (n,m) points. Normalized NIR absorption profile of (e) SaDNA and (f) $d(GT)_{20}$ dispersed HiPco SWNTs ultracentrifugation supernatant fractions. Groups of the characteristic NIR E^S_{11} peaks are deconvoluted and assigned with respect to their possible chiralities and indicated as groups in braces "{}".[13,22]

spectroscopy. From the spectra analysis of the HiPco sample, we show (1) SaDNA stabilizes dispersions of SWNTs to a level comparable to the $d(GT)_{20}$ oligomer and (2) SaDNA selectively stabilizes (6,5) tubes in the D_2O media. Semiconducting (*sem*-) SWNTs have been known to absorb and emit photons via the electronic transitions (E^S_{ii}) between valence and conduction bands[13] according to their distinct van Hove singularity (vHs).[14] Typically, SWNT PL is observed at the E^S_{11} level following the photoelectronic excitation at the first, second, and third vHs and the subsequent relaxation to the valence band edge. Thus, PL spectroscopy has been one of the primary tools for investigating *sem*-SWNTs chirality enrichment profiles by monitoring their intensity changes in absolute or relative scale.[8,15−17] Panels a−d of Figure 1 show the chirality-assigned photoluminescence excitation (PLE) emission spectra[13] acquired

from SaDNA and $d(GT)_{20}$ dispersed HiPco SWNTs,[18] which are noted as SaDNA−HiPco and $d(GT)_{20}$−HiPco, respectively. The supernatant obtained after ultracentrifugation of the SaDNA−HiPco sample shows that the relative emission intensity of (6,5) SWNT is significantly enhanced (Figure 1a), meanwhile the redispersed precipitate shows peaks corresponding to the (7,6), (8,4), and (7,5) tubes (Figure 1b). In contrast, the $d(GT)_{20}$−HiPco in both the ultracentrifuged supernatant (Figure 1c) and the redispersed precipitate fractions (Figure 1d) show similar emission profiles resulting from (7,6), (8,4), and (7,5) SWNTs. HiPco SWNTs two-dimensional (2-D) mapping PLE emission contour plots similar to those in Figure 1, panels b−d, can be found in various other references,[13,16,19] where various surfactant systems were introduced. On the basis of these results, we conclude that $d(GT)_{20}$ stabilizes HiPco SWNT without
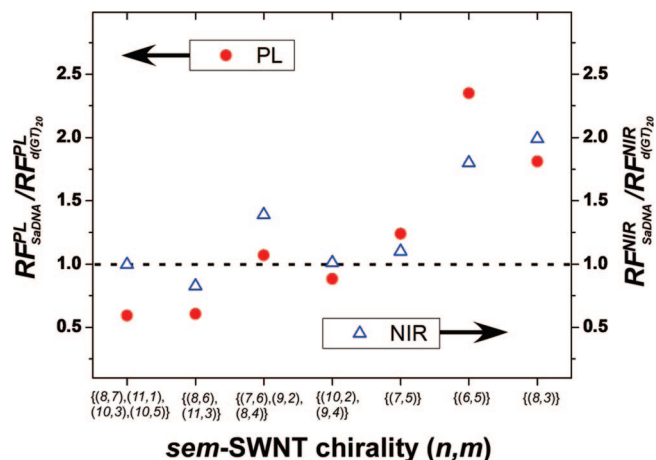
Figure 2. The relative solubility of each SWNT group from both PLE emission and NIR absorption. RF^{PL} and RF^{NIR} are the RF of each chirality group from PLE emission and NIR data, respectively. $RF^{PL}_{SaDNA}/RF^{PL}_{d(GT)_{20}}$ is calculated by averaging the RF of each (n,m) assigned from the PLE emission spectra according to the SWNT groups in NIR assignment. Placement of the data points above the broken line indicates relative enrichment of the respective chirality groups at the SaDNA−HiPco dispersion.

noticeable chirality selection by the process applied here,[18] whereas significant selective solubilization of (6,5) tube in aqueous media was observed using SaDNA. Addition of SaDNA to $d(GT)_{20}$−HiPco supernatant shows no noticeable change in the intensity and peak-position profiles of PLE emission (Figure S1a,b),[18] indicating any SaDNA-induced physicochemical effect on SWNTs, such as charge transfer,[19] is not involved in the spectral changes observed in this experiment. The SWNT−DNA dispersion exhibits neutral pH, where no redox effect is expected on the SWNT spectroscopy data.[20,21]

While the 2-D PLE emission contour plots provide the detailed information about individual *sem*-SWNT according to its chirality, NIR absorption shows peaks that are typically from several nanotubes with similar excitation energy. However, specifically for a nanotube sample with diameter similar to HiPco SWNTs, the NIR E^S_{11} does not overlap other higher electronic transitions, such as E^S_{22} and E^M_{11}, and most peaks are widely spread, enabling detailed chirality assignment of *sem*-SWNT. Thus, monitoring the enrichment profile by NIR spectroscopy can be a good secondary approach to support the PLE emission result from the HiPco nanotube sample. To avoid any spectral changes from intertube aggregation, NIR absorption spectra were obtained from the supernatant of ultracenrifuged SaDNA- and $d(GT)_{20}$-dispersed HiPco SWNTs (Figure 1e,f). Both spectra are normalized and baseline-corrected by subtracting the plasmonic and scattering lines.[22] Along with PLE emission spectra, the E^S_{11} features observed from NIR absorption of both samples are finely separated, indicating that the natural SaDNA product individually disperses SWNTs in D_2O at a level comparable to the oligo $d(GT)_{20}$. These characteristic NIR E^S_{11} peaks are deconvoluted and assigned with respect to their possible chiralities, which are based on the experimental observation and assignment from previous studies.[13,22] Groups of {(13,3), (13,5)}, {(11,6), (15,1)}, {(12,4)}, {(10,5), (10,3), (11,1), (8,7)}, {(11,3), (8,6)}, {(8,4), (9,2), (7,6)}, {(10,2), (9,4)}, {(7,5)}, {(6,5)}, and {(8,3)} SWNTs are assigned from low to high E^S_{11}. On the basis of recent

theoretically calculated PLE emission and absorption intensities,[15] the relative fraction ($RF^{PL/NIR}_{SaDNA/d(GT)_{20}}$, %)[18] of each *sem*-SWNT is calculated from PLE emission and NIR spectra (Table S1). The relative solubility of each SWNT group from both PLE emission and NIR absorption are depicted in Figure 2 by using $RF^{PL/NIR}_{SaDNA}/RF^{PL/NIR}_{d(GT)_{20}}$, where RF^{PL} and RF^{NIR} are the RFs of each chirality group from PLE emission and NIR data, respectively. $RF^{PL}_{SaDNA}/RF^{PL}_{d(GT)_{20}}$ is acquired by averaging the RF of each (n,m) assigned from the PLE emission spectra according to the SWNT groups in NIR assignment. The enrichment profile from NIR validates the relative solubility trend shown from PLE emission, where SaDNA enhances (6,5) SWNT population to the highest extent compared to the $d(GT)_{20}$ oligomer.

Circular dichroism (CD) is typically utilized to determine the solution structure of DNA forms by monitoring the intensity changes from the negative and positive peaks at 290−260 nm (P^+) and 260−230 nm (P^-), respectively.[23] The SWNT-induced structural changes of DNA using CD characteristics have been investigated by several groups.[24,25] By using heavily acid-treated commercial SWNTs, Li et al. reported carbon nanotubes induce a B−A transition of DNA. In this study, we observe that the SaDNA transitions from its native B-form to a near-A-form in the presence of HiPco SWNTs (Figure 3a). Although single stranded $d(GT)_{20}$ dispersed SWNTs have shown distinctive CD peaks from SWNT−DNA hybrid structure,[26] the spectrum observed from the SaDNA−HiPco SWNT, collected from the ultracentrifuged precipitate fraction, and redispersed in D_2O, is significantly different from $d(GT)_{20}$−HiPco SWNT dispersion and shows increase in P^+ as compared to P^-, indicating B−A transition. CD spectra of SaDNA at various ultrasonication times (Figure S3) shows no noticeable change indicating the preservation of double helix structure throughout the process.

To theoretically explore these observations, namely, that (6,5) SWNT exhibits strong association affinity to SaDNA, while no such chiral selectivity is present for $d(GT)_{20}$−SWNT complexes, classical all-atom molecular dynamics (MD) simulation was performed to compare the
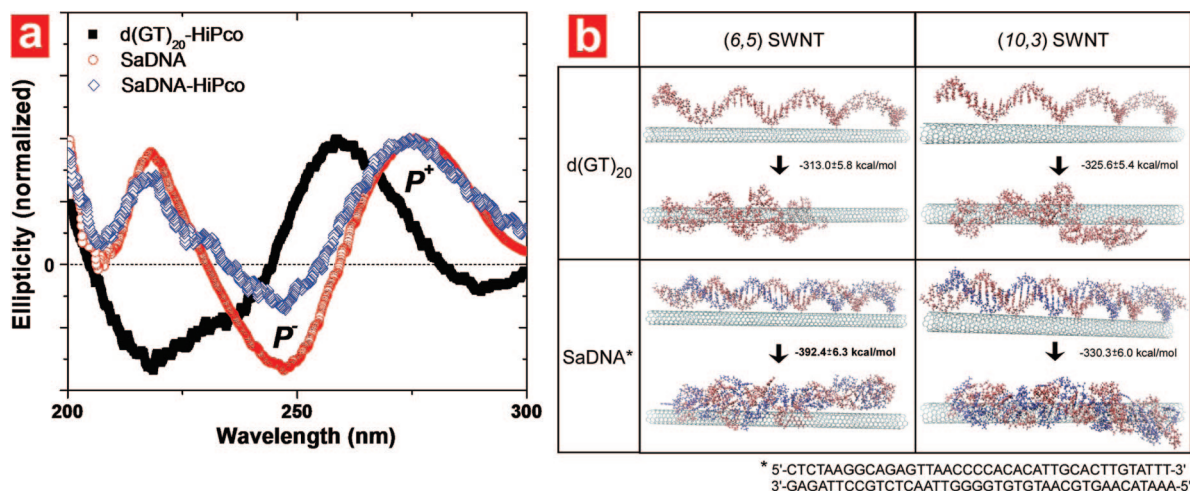
Figure 3. (a) Normalized CD spectra from SaDNA and d(GT)$_{20}$ dispersed HiPco SWNTs. SaDNA CD spectrum shows complete B-form. The negative and positive peaks at 290−260 nm and 260−230 nm are noted as P^+ and P^-, respectively. (b) Tabulated figures for the conformations of SaDNA/d(GT)$_{20}$ and (6,5)-/(10,3)-SWNT hybrids obtained from classical all-atom MD simulations. Transitions of conformations from native DNAs to energy-minimized DNA−SWNT hybrid forms are indicated as arrows along with the vdW energies between DNA and SWNT of the energy-minimized system.

relative binding affinity of single-strand d(GT)$_{20}$ and double-strand SaDNA to two representative SWNTs, (6,5) and (10,3) tubes. Since the self-assembly of DNA−SWNT complex is driven by the strong van der Waals (vdW) interaction on the interface of the nucleotides and the SWNT sidewall, and the vdW interaction is the main stabilizing force within the DNA−SWNT complex,[27,28] we calculate this vdW interaction energy between DNA and SWNT in vacuum to compare the relative binding affinity. On the basis of the known GC content of SaDNA (∼41%),[29] a sequence of DNA, consisting 40 base-pairs with length ∼13.5 nm, was randomly generated. The AMBER99 force field is used to model DNA.[30] The initial coordinates of SWNTs of length 14 nm and chirality (6,5) and (10,3) are generated by using Maruyama's wrapping program.[31] The SWNT carbon atoms are modeled by uncharged sp^2 Lennard-Jones parameters from AMBER99 force field. The DNA structures are initially placed above the SWNT by about 1.5 nm from the axis of SWNT. After energy minimization and heating up to 300 K, each system is equilibrated at least 50 ns until the total potential energy converges. By use of equilibrated trajectories, vdW interaction energies are calculated by NAMD for each system.[32]

Figure 3b shows the conformations of SaDNA− and d(GT)$_{20}$−DNA fragments with (6,5)- and (10,3)-SWNTs obtained from classical all-atom MD simulations. The single-strand d(GT)$_{20}$ rapidly wraps nanotubes from the 3′-end as shown in Figure 3b. This is in agreement with the observation from the classical all-atom MD simulations including explicit water as reported by Klein's group.[28] Figure 3b also shows double-strand DNA becomes more compact, exhibiting the A-like form. This trend fits well with the CD spectrum shift from complete B-form (the red curve in Figure 3a) to a near-A-form (the blue curve in Figure 3a). Since DNA is flexible and hydrophilic, the interactions with the stiff and hydrophobic SWNT forces hydrophilic nucleotides to choose a more compact form.

The calculated vdW interaction energies between DNA and SWNT (its absolute value is also called the total stacking

energy[28]) for the energy-minimized conformations are −392.4 ± 6.3 kcal/mol for SaDNA-(6,5), −330.3 ± 6.0 kcal/mol for SaDNA-(10,3), −312.97 ± 5.8 kcal/mol for d(GT)$_{20}$-(6,5), and −325.63 ± 5.4 kcal/mol for d(GT)$_{20}$-(10,3). SaDNA energetically prefers (6,5) to (10,3) with an energy difference of 62.1 kcal/mol. Meanwhile, d(GT)$_{20}$ shows preference toward (10,3) tube with −12.26 kcal/mol vdW energy difference, which is in the regime of error bars in the energy distributions. This theoretical calculation strongly supports the selective enrichment of (6,5)-tube with genomic SaDNA and no distinguishable observation with d(GT)$_{20}$. More extensive calculations that account not only for various other types of DNA sequences but also for additional SWNT chiralities present in the experiment, are in progress for in-depth understanding and controlling the chirality enrichment using genomic DNAs.

Radial breathing mode (RBM)[33] peaks from resonance Raman spectra (RRS) acquired using the 633 nm excitation laser line exhibit that relative intensity of SaDNA−HiPco *sem*-SWNT peaks are increased as compared to the d(GT)$_{20}$−HiPco, which shows similar RBM profiles to the as-supplied sample.[18] This indicates that SaDNA mediates preferential stabilization of *sem*-SWNTs in the aqueous supernatant, while leaving the metallic (*met*-) counterpart in the precipitate. Further detailed RRS characterization with tunable excitation laser line is required to monitor this metallicity-dependent separation. However, we chose to focus on characterizing the chirality separation of *sem*-SWNTs in this study. To further support the evidence that SaDNA significantly interacts with (6,5) SWNTs, we explore similar experiments using CoMoCat SWNTs.

CoMoCat SWNT is a well-known commercial product, where the average diameter of nanotube is ∼0.81 nm with σ of ±0.08 nm.[34] The estimated quantity of *sem*-SWNTs in CoMoCat tubes is >90% and (6,5) tube concentration reaches >50% of the total sample.[35,36] Previously, additional separation methods such as anion exchange column[11] and density gradient ultracentrifugation[6] were employed for the
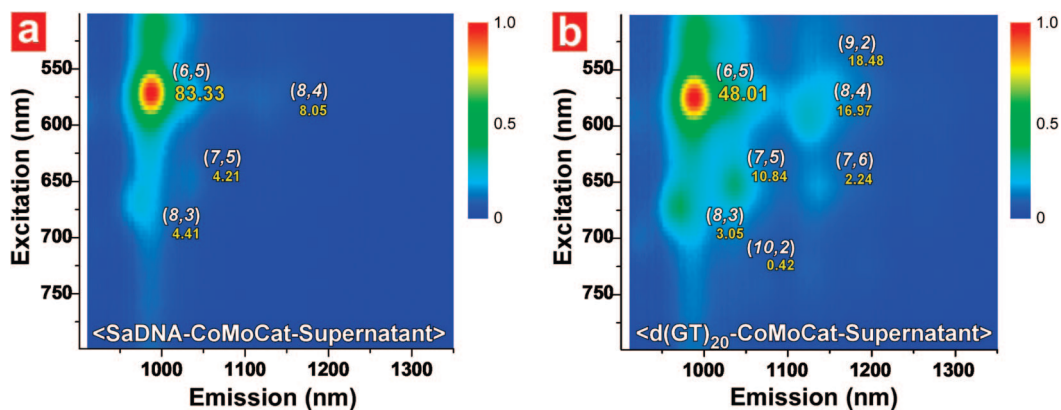
Figure 4. Normalized PLE emission contour plot of (a) SaDNA and (b) d(GT)$_{20}$ dispersed CoMoCat SWNTs from their ultracentrifugation supernatant fractions. The RF$^{PL}_{SaDNA/d(GT)_{20}}$ are shown under each chirality (n,m) assignment.

enrichment of (6,5) tube when CoMoCat SWNTs were dispersed in water using DNA oligo d(GT)$_{20}$ and sodium cholate, respectively. Here, we follow the selective stabilization trend of SaDNA toward HiPco SWNTs, and the enrichment of (6,5) SWNT from as-supplied CoMoCat samples using SaDNA as a dispersing medium in D$_2$O without the need for additional separation methods. Figure 4 shows the PLE emission profile obtained from CoMoCat SWNTs using SaDNA and d(GT)$_{20}$. The normalized PLE emission intensity from (6,5) tubes is enhanced, while other SWNT peaks are significantly diminished, as is notable from the RF changes indicated in Figure 4 next to chirality assignment. Referring to the manufacturer's specification and their PLE emission-[35] and RRS-based[36] chirality quantification studies, we estimate that the (6,5) SWNT concentration in the CoMoCat sample increased to >86% with one step of SaDNA-mediated dispersion and ultracentrifugation. The addition of ultrasonicated and ultracentrifuged SaDNA to d(GT)$_{20}$-stabilized CoMoCat SWNTs shows no noticeable change in the PLE emission profiles (Figure S1c,d),[18] confirming that the spectral difference is not due to SaDNA-induced physicochemical changes in nanotubes.

We also used *Escherichia coli* genomic DNA (EcDNA) to separate CoMoCat SWNTs (see Figure S4). Using EcDNA, we were able to observe the enrichment of (6,5) SWNTs to ~75%. One of the reasons for enhanced separation of (6,5) SWNTs using SaDNA could be attributed to its lowered GC content (41%), while in comparison, the GC content of EcDNA is around 50%. Interestingly, PLE emission spectra from CoMoCat showed that the luminescence from (6,5) tubes is relatively stronger using the lower GC content genomic SaDNA, compared to EcDNA. In addition, EcDNA exhibited lower SWNT solubilization compared to SaDNA. However, further elucidation on the separation mechanism could be addressed by identifying the DNA fragments bound to the (6,5) tubes, which is currently underway in our laboratory.

The price for d(GT)$_{20}$ is typically $25000/g and usually oligo-DNA assisted SWNT dispersion experiments are carried out with a DNA:SWNT weight ratio of 1:1, discarding the majority of unbound DNA. This poses a high price of $25000 for oligo-DNA in treating every gram of carbon

nanotubes, and thus, a cost-effective nucleic acid system is highly in demand. Genomic DNAs have emerged as a SWNT dispersing system to satisfy such demand.[37−39] NIR, PL, and MD studies reveal that SaDNA interacts with SWNT at a level comparable to the d(GT)$_{20}$ oligomer but, more importantly, exhibits (6,5)-chirality selectivity. Using SaDNA, >86% of (6,5) SWNT-enrichment is achieved using commercial CoMoCat tubes as the starting material. This finding will enable us to obtain more electronically controlled samples of SWNTs that can be used to enhance optical and semiconducting properties of nanotube-only systems[40] or nanotube composites, specifically for electronics application.[41,42] On the basis of the MD simulation-based chirality selectivity prediction, further mechanistic investigation of DNA sequences that promote selective stabilization of (6,5) SWNTs is underway in order to control and amplify the chirality enrichment from the commercial nanotube products. Clearly, the GC content of the DNA has an important role to play in SWNT separation, but just having a defined GC content might not be sufficient for chirality enrichment. DNA fragment length and sequence composition could also be important parameters to consider. In conclusion, we demonstrate a simple, scalable, and economic method for the enrichment of specific type SWNTs.

Supporting Information Available: Experimental details of SWNT−DNA dispersion, separation, and spectroscopic measurement methodologies, and details of the quantitative analysis of PLE emission and NIR spectra to assess chirality separation. This material is available free of charge via the Internet at http://pubs.acs.org.

References

(1) Chattopadhyay, D.; Galeska, I.; Papadimitrakopoulos, F. *J. Am. Chem. Soc.* **2003**, *125* (11), 3370–3375.

(2) Zheng, M.; Jagota, A.; Strano, M. S.; Santos, A. P.; Barone, P.; Chou, S. G.; Diner, B. A.; Dresselhaus, M. S.; Mclean, R. S.; Onoa, G. B.; Samsonidze, G. G.; Semke, E. D.; Usrey, M.; Walls, D. J. *Science* **2003**, *302* (5650), 1545–1548.

(3) Chen, Z.; Du, X.; Du, M. -H.; Rancken, C. D.; Cheng, H.-P.; Rinzler, A. G. *Nano Lett.* **2003**, *3* (9), 1245–1249.

(4) Krupke, R.; Hennrich, F.; Lohneysen, H. V.; Kappes, M. M. *Science* **2003**, *301* (5631), 344–347.

(5) Arnold, M. S.; Stupp, S. I.; Hersam, M. C. *Nano Lett.* **2005**, *5* (4), 713–718.

(6) Arnold, M. S.; Green, A. A.; Hulvat, J. F.; Stupp, S. I.; Hersam, M. C. *Nat. Nanotechnol.* **2006**, *1* (1), 60–65.

(7) Kim, S. N.; Luo, Z.; Papadimitrakopoulos, F. *Nano Lett.* **2005**, *5* (12), 2500–2504.

(8) Ju, S.; Doll, J.; Sharma, I.; Papadimitrakopoulos, F. *Nat. Nanotechnol.* **2008**, *3* (6), 356–362.

(9) Zheng, M.; Jagota, A.; Semke, E. D.; Diner, B. A.; McLean, R. S.; Lustig, S. R.; Richardson, R. E.; Tassi, N. G. *Nat. Mater.* **2003**, *2*, 338–342.

(10) Lu, G.; Maragakis, P.; Kaxiras, E. *Nano Lett.* **2005**, *5* (5), 897–900.

(11) Zheng, M.; Semke, E. D. *J. Am. Chem. Soc.* **2007**, *129* (19), 6084–6085.

(12) Kukovecz, A.; Kramberger, C.; Georgakilas, V.; Prato, M.; Kuzmany, H. *Eur. Phys. J. B* **2002**, *28* (2), 223–230.

(13) Bachilo, S. M.; Strano, M. S.; Kittrell, C.; Hauge, R. H.; Smalley, R. E.; Weisman, R. B. *Science* **2002**, *298* (5602), 2361–2366.

(14) Dresselhaus, M. S.; Eklund, P. C. *Adv. Phys.* **2000**, *49* (6), 705–814.

(15) Oyama, Y.; Saito, R.; Sato, K.; Jiang, J.; Samsonidze, G. G.; Gruneis, A.; Miyauchi, Y.; Maruyama, S.; Jorio, A.; Dresselhaus, G.; Dresselhaus, M. S. *Carbon* **2006**, *44* (5), 873–879.

(16) Maeda, Y.; Kanda, M.; Hashimoto, M.; Hasegawa, T.; Kimura, S.; Lian, Y.; Wakahara, T.; Akasaka, T.; Kazaoui, S.; Minami, N.; Okazaki, T.; Hayamizu, Y.; Hata, K.; Lu, J.; Nagase, S. *J. Am. Chem. Soc.* **2006**, *128* (37), 12239–12242.

(17) Li, X.; Tu, X.; Zaric, S.; Welsher, K.; Seo, W. S.; Zhao, W.; Dai, H. *J. Am. Chem. Soc.* **2007**, *129* (51), 15770–15771.

(18) Materials and methods are available as Supporting Information on http://pubs.acs.org.

(19) McDonald, T. J.; Blackburn, J. L.; Metzger, W. K.; Rumbles, G.; Heben, M. J. *J. Phys. Chem. C* **2007**, *111* (48), 17894–17900.

(20) Strano, M. S.; Huffman, C. B.; Moore, V. C.; O'Connell, M. J.; Haroz, E. H.; Hubbard, J.; Miller, M.; Rialon, K.; Kittrell, C.; Ramesh, S.; Hauge, R. H.; Smalley, R. E. *J. Phys. Chem. B* **2003**, *107* (29), 6979–6985.

(21) O'Connell, M. J.; Eibergen, E. E.; Doorn, S. K. *Nat. Mater.* **2005**, *4* (5), 412–418.

(22) Luo, Z.; Pfefferle, L. D.; Haller, G. L.; Papadimitrakopoulos, F. *J. Am. Chem. Soc.* **2006**, *128* (48), 15511–15516.

(23) Baase, W. A.; Johnson, W. C., Jr *Nucleic Acids Res.* **1979**, *6* (2), 797–814.

(24) Heller, D. A.; Jeng, E. S.; Yeung, T.-K.; Martinez, B. M.; Moll, A. E.; Gastala, J. B.; Strano, M. S. *Science* **2006**, *311* (5760), 508–511.

(25) Li, X.; Peng, Y.; Qu, X. *Nucleic Acids Res.* **2006**, *34* (13), 3670–3676.

(26) Dukovic, G.; Balaz, M.; Doak, P.; Berova, N. D.; Zheng, M.; McLean, R. S.; Brus, L. E. *J. Am. Chem. Soc.* **2006**, *128* (28), 9004–9005.

(27) Meng, S.; Maragakis, P.; Papaloukas, C.; Kaxiras, E. *Nano Lett.* **2007**, *7* (1), 45–50.

(28) Johnson, R. R.; Johnson, A. T. C.; Klein, M. L. *Nano Lett.* **2008**, *8* (1), 69–75.

(29) Macquet, J.-P.; Butour, J.-L. *Eur. J. Biochem.* **1978**, *83* (2), 375–387.

(30) Case, D. A.; Darden, T. A.; Cheatham, T. E., III; Simmerling, C. L.; Wang, J.; Duke, R. E.; Luo, R.; Merz, K. M.; Pearlman, D. A.; Crowley, M.; Walker, R. C.; Zhang, W.; Wang, B. Hayik, S.; Roitberg, A.; Seabra, G.; Wong, K. F.; Paesani, F.; Wu, X.; Brozell, S. Tsui, V.; Gohlke, H.; Yang, L.; Tan, C.; Mongan, J.; Hornak, V.; Cui, G.; Beroza, P.; Mathews, D. H.; Schafmeister, C.; Ross, W. S.; Kollman, P. A. *AMBER9*, University of California, San Francisco, 2006.

(31) http://www.photon.t.u-tokyo.ac.jp/~maruyama/wrapping3/wrapping.html.

(32) Phillips, J. C.; Braun, R.; Wang, W.; Gumbart, J.; Tajkhorshid, E.; Villa, E.; Chipot, C.; Skeel, R. D.; Kale, L.; Schulten, K. *J. Comput. Chem.* **2005**, *26* (16), 1781–1802.

(33) Kuzmany, H.; Plank, W.; Hulman, M.; Kramberger, C.; Gruneis, A.; Pichler, T.; Peterlik, H.; Kataura, H.; Achiba, Y. *Eur. Phys. J. B* **2001**, *22* (3), 307–320.

(34) Kitiyanan, B.; Alvarez, W. E.; Harwell, J. H.; Resasco, D. E. *Chem. Phys. Lett.* **2000**, *317* (3−5), 497–503.

(35) Bachilo, S. M.; Balzano, L.; Herrera, J. E.; Pompeo, F.; Resasco, D. E.; Weisman, R. B. *J. Am. Chem. Soc.* **2003**, *125* (37), 11186–11187.

(36) Jorio, A.; Santos, A. P.; Ribeiro, H. B.; Fantini, C.; Souza, M.; Vieira, J. P. M.; Furtado, C. A.; Jiang, J.; Saito, R.; Balzano, L.; Resasco, D. E.; Pimenta, M. A. *Phys. Rev. B* **2005**, *72* (7), 075207.

(37) Barisci, J. N.; Tahhan, M.; Wallace, G. G.; Badaire, S.; Vaugien, T.; Maugey, M.; Poulin, P. *Adv. Func. Mater.* **2004**, *14* (2), 133–138.

(38) Gigliotti, B.; Sakizzie, B.; Bethune, D. S.; Shelby, R. M.; Cha, J. N. *Nano Lett.* **2006**, *6* (2), 159–164.

(39) Asada, Y.; Dohi, H.; Kuwahara, S.; Sugai, T.; Kitaura, R.; Shinohara, H. *Nano* **2007**, *2* (5), 295–299.

(40) LeMieux, M. C.; Roberts, M.; Barman, S.; Jin, Y. W.; Kim, J. M.; Bao, Z. *Science* **2008**, *321* (5885), 101–104.

(41) Hagen, J. A.; Li, W.; Steckl, A. J.; Grote, J. G. *Appl. Phys. Lett.* **2006**, *88* (17), 171109.

(42) Singh, B.; Sariciftci, N. S.; Grote, J. G.; Frank, K. H. *J. Appl. Phys.* **2006**, *100* (2), 024514.

NL802332V